# Plastic-Filled Dual-Polarized Lens Antenna for Beam-Switching in the *Ka*-Band

Resti Montoya Moreno, Juha Ala-Laurinaho, and Ville Viikari, *Senior Member, IEEE*

***Abstract*—This letter presents a circular lens antenna for wide-angle beam steering and for dual-polarized operation at millimeter-wave (mm-wave) frequencies (27–30 GHz). The lens consists of a dielectric disc and two parallel plates, whose vertical spacing is varied linearly to achieve a suitable effective refraction index profile for the polarization parallel to the plates. The desired refraction profile is that of the Luneburg lens. The variation in plate spacing has negligible effect on the polarization perpendicular to the plates, and therefore, the dielectric material is selected such that the circular shape of the lens approximates the dimensions of the extended hemispherical lens. This way, the lens provides focusing or collimation for both linear polarizations. The lens is fed with square waveguides supporting both polarizations. Several feeding waveguides allow beam switching over a wide angular range. The designed lens antenna was fabricated, and the simulation and measurement results agree well and show that the proposed antenna concept is a valid solution for the upcoming 5G technologies, for instance as the access-point antenna. The antenna provides a $\pm 50^{\circ}$ beam-scanning range in both polarizations, and the realized gain is mostly between 9 and 12 dBi for the main beam. The measured reflection coefficient is mainly below $-10$ dB for both polarizations across the whole frequency band.**

***Index Terms*—Access point, base station, beam switching, lens antenna, millimeter-wave (mm-wave), waveguide, 5G.**

## I. Introduction

CURRENT mobile communication networks cannot fully meet the demands of future applications, such as the Internet of Things, machine-to-machine communication, self-driving cars, or augmented reality. The exponential increase in the amount of connected devices is creating a need for the development of the fifth generation of mobile communication networks (5G). In order to achieve increased data rates, millimeter-wave (mm-wave) bands, such as those in the 20–80 GHz range, have attracted a lot of attention and are currently being studied [1], [2].

Millimeter-wave antennas should generally be beam-steerable with a relatively large beam-steering range for maximal coverage. Dual-polarized operation is additionally desired for improved link reliability and capacity.

Manuscript received August 5, 2019; accepted September 3, 2019. Date of publication September 17, 2019; date of current version December 19, 2019. *(Corresponding author: Resti Montoya Moreno.)*

The authors are with the Department of Electronics and Nanoengineering, School of Electrical Engineering, Aalto University, 00076 Espoo, Finland (e-mail: resti.montoyamoreno@aalto.fi; juha.ala-laurinaho@aalto.fi; ville.viikari@aalto.fi).

Digital Object Identifier 10.1109/LAWP.2019.2939901

Different solutions have been studied in recent years, some of the most studied being leaky-wave antennas [3], reflectarrays [4], phased arrays [5], [6], and lens antennas [7]–[20]. Sánchez-Escuderos *et al.* [3] achieve a really low reflection coefficient and high gain in their antenna. However, its beam cannot be steered at a single frequency and rather points to a different direction for different frequencies. Karnati *et al.* [4] present an antenna design with a very compact structure. Unfortunately, relatively high losses decrease the achieved realized gain. Even though they are able to achieve continuous beam steering, the range is only $\pm 25^{\circ}$. A very interesting phased array is presented in [5]. The achieved gain and total efficiency are very good, and the beam can be steered up to $70^{\circ}$. However, only simulation results are presented, and no feeding network is included in this letter. The phased array antenna presented in [6] exhibits excellent performance, but its transmission losses are relatively high.

Lens antennas have commonly been used at high frequencies, but their spherical shape makes them bulky and unappealing for 5G portable devices or access points. In order to make the lens antennas practical and to reduce their dimensions, they can be sliced in the vertical plane, forming a parallel-plate structure. However, the loss of symmetry in one plane makes the design of dual-polarized lens antennas challenging. Hua *et al.* [18] achieve wide-angle beam scanning, low reflection coefficient, and high realized gain in the 29–32 GHz range. However, the antenna operates at a single polarization. A cylindrical Luneberg lens antenna is presented in [19]. Low sidelobe level and high gain are achieved in the 26.5–37 GHz range, but the beam-steering capabilities are not shown. In [20], a two-dimensional cylindrical lens is presented. High realized gain in the $\pm 30^{\circ}$ range is achieved for single-polarized operation. This interesting study, however, is limited to simulations.

We propose a novel dual-polarized lens structure that combines an array of dual-polarized square waveguides and a flat circular lens. The feeding network presents low losses, and the circular shape of the lens enables wide beam scanning in the horizontal plane by beam switching. Fan-shaped beams provide wide coverage in the elevation plane. The result is a high-gain, small-size, and easy-to-manufacture structure that can be integrated into portable devices or used as a 5G access point that operates in the 27–30 GHz range.

This letter is organized as follows. In Section II, we describe the mm-wave lens antenna and its feeding structure. Section III introduces the manufactured prototype. Simulation and measurement results are compared in Section IV. Finally, conclusions are drawn in Section V.

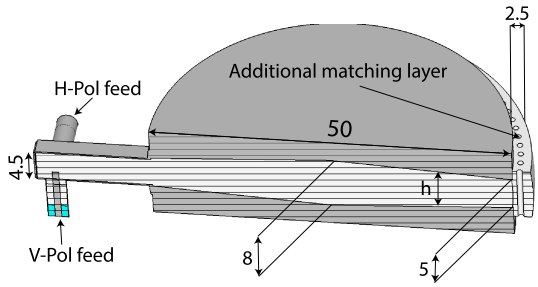


Fig. 1. Transversal cut of the proposed lens antenna. All dimensions are in millimeters.

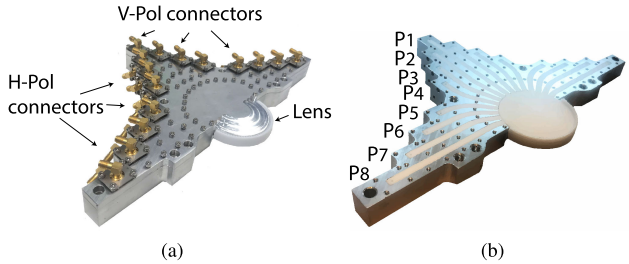


Fig. 2. Prototype lens antenna (a) with the top metal cover and (b) without the top metal cover.

## II. Dual-Polarized Dielectric-Filled Circular Lens Antenna

The proposed structure can be divided into two main parts: the feeding structure and the lens antenna.

*1) Feeding Structure:* The feeding structure used in the design consists of an array of square waveguides. They have low losses and are convenient to fabricate. We chose square waveguides as they support both polarizations, unlike the commonly used rectangular waveguides with 2:1 ratio between height and width. The number of square waveguides feeding the lens can be increased in order to achieve a wide beam-scanning range through beam switching.

The cutoff frequency of a waveguide is given by [21]

$$f_{\mathrm{c}} = \frac{1}{2\pi\sqrt{\epsilon\mu}}\sqrt{\left(\frac{m\pi}{a}\right)^2 + \left(\frac{n\pi}{b}\right)^2} \tag{1}$$

where $\epsilon$ is the permittivity, $\mu$ is the permeability, $a$ and $b$ are the waveguide dimensions, and $m$ and $n$ correspond to the order of the propagated TE or TM mode.

Fig. 1 shows the proposed Teflon-filled waveguide having dimensions $4.5 \times 4.5$ mm$^2$, implying that its cutoff frequency is 23 GHz.

*2) Lens Antenna:* Since the lens height is restricted, it behaves as a parallel-plate waveguide filled with Teflon. A challenge in this kind of a lens is that the loss of symmetry makes it difficult to ensure that the horizontal and vertical polarizations propagate and achieve collimation in a similar way. A simple linear loft in the lens going from the edge to the center has been proposed as a solution in [17]–[19]. This loft improves the $\mathrm{TE}_{01}$ (polarization parallel to plates) operation since it helps to achieve the Luneburg's effective index of refraction without using multiple dielectric materials with different permittivities. The refractive index ($n$) in a parallel-plate waveguide for the fundamental mode $\mathrm{TE}_{01}$ is

$$n = \frac{k}{k_0} = \sqrt{1 - \left(\frac{\lambda}{2h}\right)^2} \tag{2}$$

where $h$ is the spacing between the parallel plates and $\lambda$ is the wavelength in the dielectric. The refractive index can be, therefore, modified by adjusting $h$ in order to achieve the Luneburg's refractive index, which is defined by the following formula [22]:

$$n = N_0\sqrt{2 - \delta r^2} \tag{3}$$

where $r$ is the normalized radius and $N_0$ and $\delta$ are two adjustable parameters. When $N_0$ and $\delta$ are reduced to one, (3) reduces to Luneberg's law. The fundamental mode $\mathrm{TE}_{01}$ is excited between the parallel plates, when the distance between them $h$ is set between $\lambda_{\mathrm{g}}/2 < h < \lambda_{\mathrm{g}}$. As shown in Fig. 1, $h$ varies between 5 and 8 mm.

For the perpendicularly polarized fields, TEM, the lens behaves like an extended hemispherical lens, where Teflon ($\epsilon_r = 2.1$) presents a close to optimal value for the permittivity in order to obtain the maximum gain.

An extra layer of shaped Teflon is added to the outer surface of the lens. This matching layer has an effective permittivity of $\epsilon_r = 1.5$, which creates a smooth transition between air and Teflon, thus reducing reflections. In order to decrease the effective permittivity of Teflon, some of the material was extracted by drilling holes in the layer. The volume that should be removed is calculated using the Maxwell–Garnett equation [23]

$$\frac{\epsilon_{\mathrm{eff}} - \epsilon_{\mathrm{m}}}{\epsilon_{\mathrm{eff}} + 2\epsilon_{\mathrm{m}}} = \delta_{\mathrm{i}}\frac{\epsilon_{\mathrm{i}} - \epsilon_{\mathrm{m}}}{2\epsilon_{\mathrm{i}} + 2\epsilon_{\mathrm{m}}} \tag{4}$$

where $\epsilon_{\mathrm{eff}}$ is the effective permittivity, $\epsilon_{\mathrm{i}}$ is the permittivity of the material included (air), $\epsilon_{\mathrm{m}}$ is the main material (Teflon), and $\delta_{\mathrm{i}}$ is the proportion by volume of the included material. The matching layer extends 2.5 mm over the lens diameter.

## III. Lens Prototype

After determining all the dimensions with the 3-D electromagnetic simulation software CST, the prototype lens, shown in Fig. 2(a), was manufactured in order to verify the functioning of the proposed antenna concept.

In order to study the maximum beam-scanning range, a total of 15 square waveguide elements are used to feed the lens. The coaxial feed design consists of two probes, one for each polarization. The vertical and horizontal probes are introduced 1.2 and 1.4 mm, respectively, inside the waveguide, slightly offset from each other. Hence, the vertical and horizontal probes are placed 2.6 and 3 mm, respectively, from the beginning of the waveguide.

The prototype consists of the metallic body, the lens, and the connectors. As shown in Fig. 2(b), the main body is made of two pieces in order to enable filling the waveguides with Teflon and

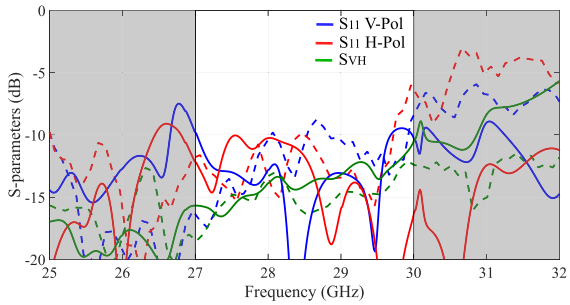


Fig. 3. Reflection coefficients and coupling between both feeds ($S_{VH}$) for port $P_1$ of the proposed antenna. Solid lines correspond to the simulated values, and dashed to the measured ones.

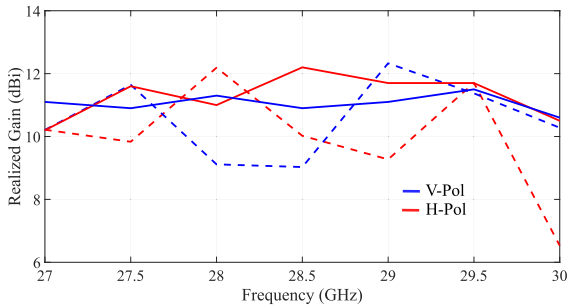


Fig. 4. Measured and simulated peak realized gain for the proposed lens antenna fed from port $P_1$. Solid lines correspond to the simulated values, and dashed to the measured ones.

replacing the lens, which is made from a separate shaped piece of Teflon. The resulting structure is bulky due to the 30 large SSMA connectors needed to test all the beams at both orthogonal polarizations. In a real application, the structure could be more integrated so that its total size is reduced significantly.

## IV. Results

The measurement results presented in this section were obtained using a vector network analyzer (VNA) and a near-field scanner. The results from port 8 ($P_8$, the widest beam-scanning angle) are not included since this port did not work as intended. The simulated and measured $S$-parameters for port $P_1$ are shown in Fig. 3. Matching levels are primarily below $-10$ dB for both polarizations in the frequency range of operation. Coupling between both polarizations is below $-13$ dB in the 27–30 GHz frequency range.

Fig. 4 compares the measured and simulated realized gain values achieved for port $P_1$ for both vertical and horizontal polarizations, respectively. The realized gain is mainly between 9 and 12 dBi in the frequency band of interest. Fig. 5 shows the measured 3-D boresight radiation pattern for port $P_1$ for vertical and horizontal polarizations, respectively, at 29 GHz.

Beam-scanning capabilities are of crucial importance in mm-wave devices, where a wider scanning range means larger coverage and better service for users. Figs. 6 and 7 show the beam-scanning capabilities at 29 GHz for vertical and horizontal polarizations, respectively. The beam can be scanned up to $\pm 50^\circ$.

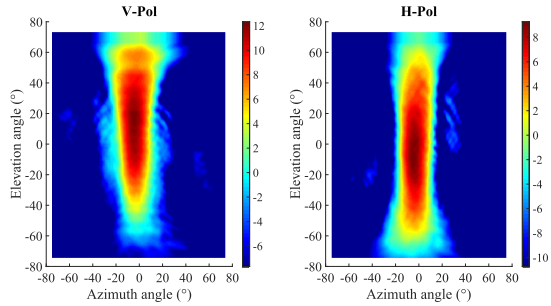


Fig. 5. Measured 3-D radiation pattern of the proposed lens antenna for $P_1$ at 29 GHz for V-Pol and H-Pol, respectively. Values in dBi.

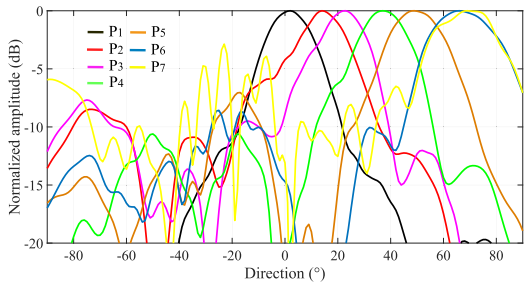


Fig. 6. Measured normalized radiation patterns in the azimuth plane for vertical polarization at 29 GHz.

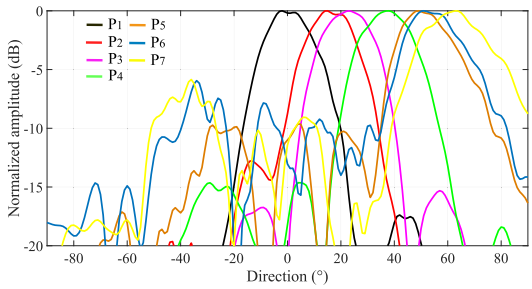


Fig. 7. Measured normalized radiation patterns in the azimuth plane for horizontal polarization at 29 GHz.

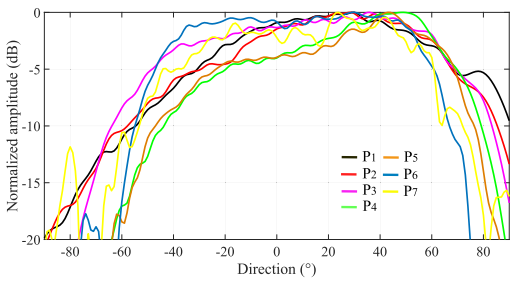


Fig. 8. Measured normalized radiation pattern in the elevation plane in the vertical polarization for the direction of the main beam at 29 GHz.

Figs. 8 and 9 show the measured and normalized elevation cut for the main beam for each port. Tables I and II show the realized gain and beam direction for each port for the vertical and horizontal polarizations for different frequencies.

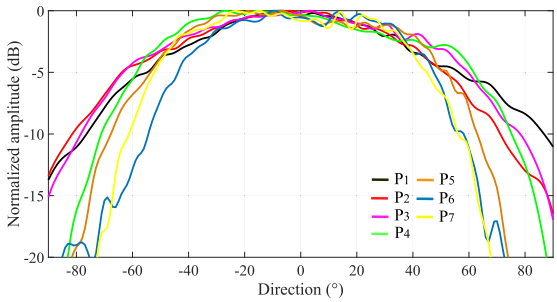


Fig. 9. Measured normalized radiation pattern in the elevation plane in the horizontal polarization for the direction of the main beam at 29 GHz.

TABLE I
SIMULATED AND MEASURED ANTENNA CHARACTERISTICS IN THE VERTICAL POLARIZATIONS AT 27, 29, AND 30 GHZ

| Port | V-Pol angle (°) sim./meas. | | | V-Pol Gain (dBi) sim./meas. | | |
|---|---|---|---|---|---|---|
| | 27 | 29 | 30 | 27 | 29 | 30 |
| P1 | 0/2 | 0/2 | 0/1 | 11.2/10.2 | 11.1/12.3 | 10.6/10.3 |
| P2 | 10/16 | 10/14 | 10/12 | 11.1/11 | 11/12.4 | 10.7/10.7 |
| P3 | 18/24 | 19/23 | 19/24 | 10.5/11.7 | 11/11.4 | 10.4/11.5 |
| P4 | 27/35 | 28/37 | 29/38 | 10.9/12.1 | 11.3/12 | 10.712.3 |
| P5 | 38/49 | 39/49 | 38/52 | 10.4/11.7 | 11/10.6 | 10.2/11.8 |
| P6 | 47/59 | 48/66 | 48/64 | 9.6/10.4 | 10/10.6 | 9.8/9.3 |
| P7 | 58/68 | 58/69 | 57/75 | 9.1/4.5 | 9.4/5.4 | 9/4 |

TABLE II
SIMULATED AND MEASURED ANTENNA CHARACTERISTICS IN THE HORIZONTAL POLARIZATIONS AT 27, 29, AND 30 GHZ

| Port | H-Pol angle (°) sim./meas. | | | H-Pol Gain (dBi) sim./meas. | | |
|---|---|---|---|---|---|---|
| | 27 | 29 | 30 | 27 | 29 | 30 |
| P1 | 0/0 | 0/2 | 0/-1 | 10/10.2 | 11.7/9.3 | 10.4/6.8 |
| P2 | 11/13 | 11/15 | 10/11 | 11.2/10.6 | 11.3/10.6 | 10.5/9.3 |
| P3 | 22/25 | 21/23 | 21/22 | 11.1/10 | 11/12.3 | 11.2/11.9 |
| P4 | 30/38 | 31/38 | 32/36 | 10.6/9.3 | 11.4/11.8 | 10.8/11.7 |
| P5 | 43/51 | 41/49 | 41/49 | 9.8/7.6 | 11.5/8.1 | 9.3/7.9 |
| P6 | 52/57 | 51/53 | 50/53 | 9.3/8.1 | 9.4/9 | 10/8.6 |
| P7 | 60/61 | 60/63 | 60/62 | 8.1/4.4 | 9.5/5.1 | 8.8/4.3 |

The simulated and measured results are generally in good agreement. However, during the assembly process, a small possible air gap was noticed between the end of the waveguides and the lens. The air gap is hidden between the plates when the lens is closed, and therefore, its exact magnitude cannot be quantified. Moreover, and due to the prototype structure, it is not possible to add any additional piece of Teflon to eliminate it. Measurement results show relatively large sidelobes. Fig. 10 shows the *E*-field distribution inside the lens. For large scanning angles, the metallic edges of the lens partially block and diffract the energy, reducing the beam-scanning range and creating sidelobes toward the opposite direction.

Table III compares the proposed design with similar solutions from the literature. The performance of the proposed solution

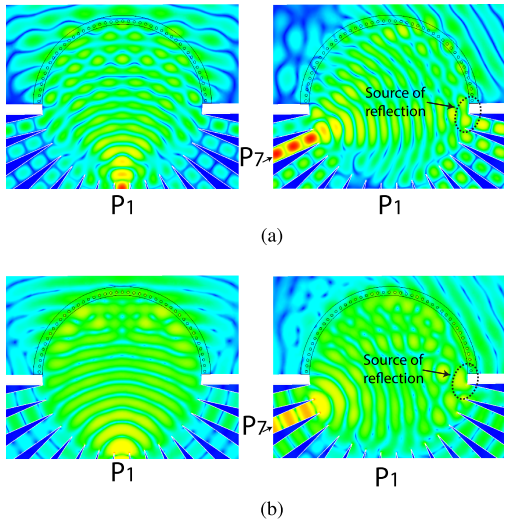


Fig. 10. *E*-field distribution when ports $P_1$ and $P_7$ are fed for (a) vertical and (b) horizontal polarization.

TABLE III
COMPARISON OF THIS LETTER WITH SIMILAR DESIGNS IN THE LITERATURE

| Ref. | Lens diameter (mm) | Gain (dBi) | Bandwidth (GHz) | Scanning angle (°) | Dual-Polarized |
|---|---|---|---|---|---|
| [18] | 100 | 15-17 | 29-32 | ±80 | No |
| [19] | 100 | 15-19 | 26.5-37 | N/A | No |
| [20] | 98.4 | 19 | 28 | ±30 | No |
| **This work** | **50** | **7-12** | **27-30** | **±50** | **Yes** |

is comparable to the other designs. However, this is the only solution that provides dual-polarized operation.

## V. CONCLUSION

A dual-polarized circular-modified lens antenna is presented in this letter. The lens behaves as a Luneburg lens for the parallelly polarized field and as an extended hemispherical lens for the perpendicularly polarized field. The device operates properly in the 27–30 GHz band, which has recently attracted a lot of attention. The reflection coefficient is primarily below −10 dB over the entire band, and the beam scanning achieved by beam switching is ±50°. The realized gain is mainly above 9 dBi over the whole frequency band. The proposed structure enables dual-polarized operation in a packed structure. The low-profile antenna described in this letter can be scaled in order to operate at different frequencies, and the feeding network can be varied according to the needs of the application. For example, a more compact feeding network could be implemented in a printed circuit board using microstrip-to-waveguide transitions instead of bulky coaxial connectors. This antenna can be potentially used in 5G mm-wave access points and 60 GHz WiFi.

## ACKNOWLEDGMENT

The authors would like to thank E. Kahra for his help in manufacturing the prototype.

## REFERENCES


[1] *Looking Ahead to 5G*, Nokia, Espoo, Finland, 2014.

[2] *5G Spectrum*, Public Policy Position, Huawei, Shenzhen, China, 2018.

[3] D. Sánchez-Escuderos, M. Ferrando-Bataller, J. I. Herranz, and M. Cabedo-Fabrés, "Periodic leaky-wave antenna on planar goubau line at millimeter-wave frequencies," *IEEE Antennas Wireless Propag. Lett.*, vol. 12, pp. 1006–1009, 2013.

[4] K. K. Karnati, M. E. Trampler, and X. Gong, "A monolithically BST-integrated $k_a$-band beamsteerable reflectarray antenna," *IEEE Trans. Antennas Propag.*, vol. 65, no. 1, pp. 159–166, Jan. 2017.

[5] N. Ojaroudiparchin, M. Shen, and G. F. Pedersen, "8 $\times$ 8 planar phased array antenna with high efficiency and insensitivity properties for 5G mobile base stations," in *Proc. 10th Eur. Conf. Antennas Propag.*, Apr. 2016, pp. 1–5.

[6] R. Valkonen, "Compact 28 GHz phased array antenna for 5G access," in *Proc. IEEE Microw. Theory Techn. Soc. Int. Microw. Symp.*, Jun. 2018, pp. 1334–1337.

[7] A. E. I. Lamminen *et al.*, "Beam-switching dual-spherical lens antenna with low scan loss at 71–76 GHz," *IEEE Antennas Wireless Propag. Lett.*, vol. 17, no. 10, pp. 1871–1875, Oct. 2018.

[8] S. K. Karki, J. Ala-Laurinaho, V. Viikari, and R. Valkonen, "Lens antenna design for E-band point-to-point radio links," in *Proc. Prog. Electromagn. Res. Symp.*, May 2017, pp. 1625–1631.

[9] Y. Su and Z. N. Chen, "A flat dual-polarized transformation-optics beam-scanning Luneburg lens antenna using PCB-stacked gradient index metamaterials," *IEEE Trans. Antennas Propag.*, vol. 66, no. 10, pp. 5088–5097, Oct. 2018.

[10] J. Ala-Laurinaho, A. Karttunen, and A. V. Räisänen, "A mm-wave integrated lens antenna for E-band beam steering," in *Proc. 9th Eur. Conf. Antennas Propag.*, Apr. 2015, pp. 1–2.

[11] A. Karttunen, J. Ala-Laurinaho, R. Sauleau, and A. V. Räisänen, "2D beam-steering with non-symmetrical beam using non-symmetrical integrated lens antenna," in *Proc. 6th Eur. Conf. Antennas Propag.*, Mar. 2012, pp. 2976–2980.

[12] A. Artemenko, A. Mozharovskiy, A. Sevastyanov, V. Ssorin, and R. Maslennikov, "High gain lens antennas for 71–86 GHz point-to-point applications," in *Proc. Eur. Microw. Conf.*, Oct. 2013, pp. 361–364.

[13] A. Artemenko, A. Mozharovskiy, A. Maltsev, R. Maslennikov, A. Sevastyanov, and V. Ssorin, "2D electronically beam steerable integrated lens antennas for mm-wave applications," in *Proc. 42nd Eur. Microw. Conf.*, Oct. 2012, pp. 213–216.

[14] J. Ala-Laurinaho, A. Karttunen, J. Säily, A. Lamminen, R. Sauleau, and A. V. Räisänen, "mm-wave lens antenna with an integrated LTCC feed array for beam steering," in *Proc. 4th Eur. Conf. Antennas Propag.*, Apr. 2010, pp. 1–5.

[15] M. K. Saleem, H. Vettikaladi, M. A. S. Alkanhal, and M. Himdi, "Lens antenna for wide angle beam scanning at 79 GHz for automotive short range radar applications," *IEEE Trans. Antennas Propag.*, vol. 65, no. 4, pp. 2041–2046, Apr. 2017.

[16] Y. F. Wu, Y. J. Cheng, and Z. X. Huang, "Ka-band near-field-focused 2-D steering antenna array with a focused Rotman lens," *IEEE Trans. Antennas Propag.*, vol. 66, no. 10, pp. 5204–5213, Oct. 2018.

[17] C. Hua, X. Wu, and W. Wu, "A millimeter-wave cylindrical modified Luneberg lens antenna," in *IEEE Microw. Theory Techn. Soc. Int. Microw. Symp. Dig.*, Jun. 2012, pp. 1–3.

[18] C. Hua, X. Wu, N. Yang, and W. Wu, "Air-filled parallel-plate cylindrical modified Luneberg lens antenna for multiple-beam scanning at millimeter-wave frequencies," *IEEE Trans. Microw. Theory Techn.*, vol. 61, no. 1, pp. 436–443, Jan. 2013.

[19] X. Wu and J. Laurin, "Fan-beam millimeter-wave antenna design based on the cylindrical Luneberg lens," *IEEE Trans. Antennas Propag.*, vol. 55, no. 8, pp. 2147–2156, Aug. 2007.

[20] S. Shad, S. Kausar, and H. Mehrpouyan, "Waveguide-fed lens based beam-steering antenna for 5G wireless communications," in *Proc. IEEE Int. Symp. Antennas Propag. USNC-URSI Radio Sci. Meeting*, Jul. 2019.

[21] D. M. Pozar, *Microwave Engineering*, 4th ed. Hoboken, NJ, USA: Wiley, 2011.

[22] E. W. Marchand, *Gradient Index Optics*, New York, NY, USA: Academic, 1978.

[23] T. C. Choy, *Effective Medium Theory: Principle and Applications*. Oxford, U.K.: Clarendon, 1999.